ELSEVIER

Chemical Engineering Science 62 (2007) 2096–2108

Chemical
Engineering Science

www.elsevier.com/locate/ces

Hydrodynamics and mass transfer characteristics in gas–liquid flow through a rectangular microchannel

Jun Yue[a,b,c], Guangwen Chen[a,*], Quan Yuan[a], Lingai Luo[b], Yves Gonthier[b]

[a]*Dalian Institute of Chemical Physics, Chinese Academy of Sciences, Dalian 116023, China*
[b]*LOCIE, Université de Savoie, Campus Scientifique, Savoie Technolac 73376, Le Bourget-du-Lac cedex, France*
[c]*Graduate University, Chinese Academy of Sciences, Beijing 100039, China*

Received 14 March 2006; received in revised form 3 October 2006; accepted 21 December 2006
Available online 17 January 2007

Abstract

Researches on two-phase transfer and reaction processes in microchannnels are important to the design of multiphase microchemical systems. In the present work, hydrodynamics and mass transfer characteristics in cocurrent gas–liquid flow through a horizontal rectangular microchannel with a hydraulic diameter of 667 μm have been investigated experimentally. Liquid side volumetric mass transfer coefficients were measured by absorbing pure CO_2 into water and a 0.3 M $NaHCO_3$ / 0.3 M Na_2CO_3 buffer solution. Interfacial areas were determined by absorbing pure CO_2 into a 1 M NaOH solution. Two-phase flow patterns and pressure drop data were also obtained and analyzed. This paper shows that two-phase frictional pressure drop in the microchannel can be well predicted by the Lockhart–Martinelli method if we use a new correlation of C value in the Chisholm's equation. Liquid side volumetric mass transfer coefficient and interfacial area as high as about $21\,s^{-1}$ and $9000\,m^2/m^3$, respectively, can be achieved in the microchannel. Generally, liquid side volumetric mass transfer coefficient increases with the increasing superficial liquid or gas velocity, which can be described satisfactorily by the developed empirical correlations. A comparison of mass transfer performance among different gas–liquid contactors reveals that the gas–liquid microchannel contactor of this study can provide at least one or two orders of magnitude higher liquid side volumetric mass transfer coefficients and interfacial areas than the others.

Keywords: Microchannel; Multiphase flow; Mass transfer; Absorption; Pressure drop; Process intensification

1. Introduction

During the last decade, microreaction technology has experienced spectacular development and has been used in a variety of applications by chemists and chemical engineers, which mainly results from numerous distinguished advantages offered by this technology such as enhanced heat and mass transfer, improved chemistry, easy scaling up and increased safety (Ehrfeld et al., 2000; Jähnisch et al., 2004; Jensen, 2001; Kolb and Hessel, 2004; Watts and Haswell, 2005). However, for rational designs of such microchemical systems, fundamental issues related to characteristics of transfer and reaction processes in microchannels should be investigated before.

Gas–liquid contacting is involved in many industrially relevant operations. When these processes are operated in microchannels, gas–liquid interfacial areas are expected to be very large due to the dramatic reduction of characteristic dimension to micron scale, thus gas–liquid mass transfer rates are greatly increased, which can benefit such applications as gas–liquid catalytic hydrogenation, direct fluorination and gas absorption (de Mas et al., 2003; Hessel et al., 2005; Jähnisch et al., 2000; Kobayashi et al., 2004; Löb et al., 2004; Tegrotenhuis et al., 2000; Yeong et al., 2004). For example, Jähnisch et al. (2000) have successfully tested gas/liquid microreactors, namely two micro bubble columns and a falling film microreactor, for the direct fluorination of toluene. The formation of extra thin liquid layers in microchannels resulted in very large interfacial areas, e.g. up to about $20,000\,m^2/m^3$, which exceeded those of laboratory bubble columns and other conventional industrial gas–liquid contactors by at least one or two orders of magnitude. Integrated with mini heat exchangers, these gas–liquid microchemical systems could safely produce mono-fluorinated toluene with much higher space–time yields.

---

* Corresponding author. Tel.: +86 411 8437 9031; fax: +86 411 8469 1570.
E-mail address: gwchen@dicp.ac.cn (G. Chen).

0009-2509/$ - see front matter © 2007 Elsevier Ltd. All rights reserved.
doi:10.1016/j.ces.2006.12.057

Gas–liquid mass transfer operations or reactions are always closely interrelated with two-phase flow patterns. In a microchannel, the predominance of interfacial forces will cause gas–liquid two-phase flow characteristics (flow pattern and its transition rule, pressure drop characteristics) behave very differently from those in conventional large-sized channels, as reported by many authors (Chung and Kawaji, 2004; Kawahara et al., 2002; Serizawa et al., 2002; Zhao and Bi, 2001a). As a result, gas–liquid mass transfer behaviors associated with these flow patterns in the microchannel may be different from those in large channels. It means that the applicability of the currently available correlations on mass transfer in gas–liquid flow in large tubes should be further examined in the microchannel. Newly designed experiments should be conducted to investigate gas liquid mass transfer characteristics in the microchannel.

So far, to the best of knowledge, detailed experimental results on mass transfer in gas–liquid flow in microchannels are scarce. Therefore, the aim of this work is experimental measurement of mass transfer characteristics in a rectangular microchannel with a hydraulic diameter of 667 μm. First, both physical and chemical methods were employed to investigate mass transfer parameters (liquid side volumetric mass transfer coefficient, interfacial area and liquid side mass transfer coefficient) in the microchannel. Two-phase flow patterns and pressure drop data under these experimental conditions were also examined. Then the influence of operational conditions was discussed and new correlations were proposed. Finally, a comparison of mass transfer performance among different gas–liquid contactors was performed to reveal the superiority of the gas–liquid microchannel contactor.

2. Experimental apparatus and procedure

2.1. Gas–liquid microchannel contactor specification

To measure mass transfer characteristics in the microchannel accurately, two gas–liquid microchannel contactors micromachined on the polymethyl methacrylate (PMMA) substrate were used in this work. As shown in Fig. 1(a), the first contactor mainly contains a Y-type rectangular microchannel with a hydraulic diameter of 667 μm (1000 μm deep, 500 μm wide). Both the gas and liquid inlet sections have lengths of 1.5 cm and the angle between them is 60°. The straight section in the microchannel for gas–liquid contacting is 4.8 cm long. In order to form a closed microchannel, the microchannel plate was covered with a piece of transparent adhesive tape. Then a smooth PMMA plate was placed on the top. The two plates were clamped together tightly through the bolting holes distributing symmetrically on the peripheries. Necessary tubings can be connected to the contactor through inlet and outlet plenums providing accesses to fluids. This contactor will be referred to as SMC I. The second contactor shown in Fig. 1(b) was used for the elimination of end effects and will be termed hereafter as SMC II. Compared with Fig. 1(a), it can be seen that in SMC II the two-phase inlet region and the outlet zone corresponding to SMC I are directly connected while the straight microchannel section for gas–liquid contacting is absent.

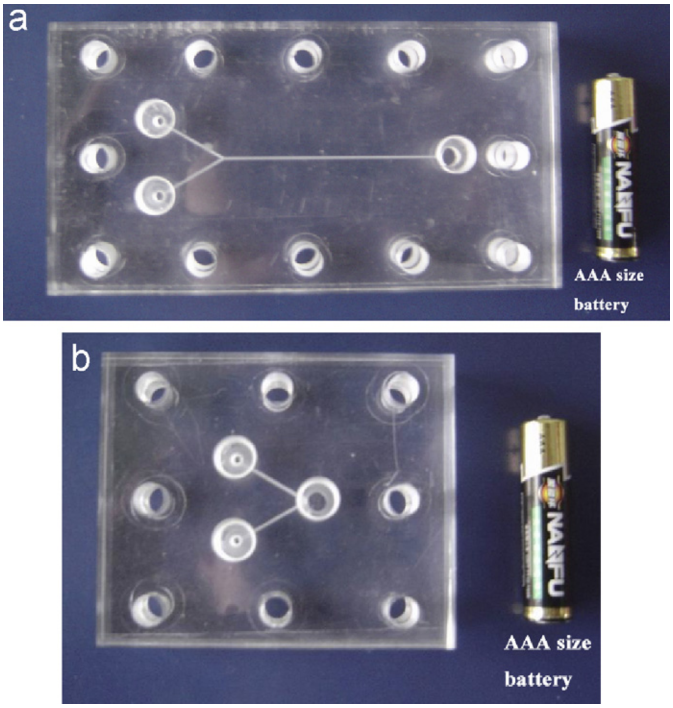

Fig. 1. Pictures of the gas–liquid microchannel contactors: (a) SMC I; (b) SMC II.

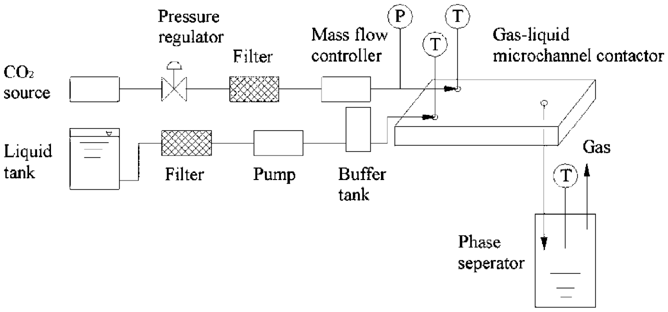

Fig. 2. Experimental setup for physical or chemical mass transfer study in the gas–liquid microchannel contactor.

2.2. Experimental setup

To characterize gas–liquid mass transfer in the microchannel, both physical and chemical mass transfer experiments were conducted. A schematic diagram of the test facility for these experiments is presented in Fig. 2.

2.2.1. Physical mass transfer experiments

As shown in Fig. 2, pure CO_2 from a gas cylinder was conveyed by a pressure regulator and was forced to flow through a filter to remove possible contaminations. Then a mass flow controller was used to ensure a constant gas flow rate into

SMC I. The gas inlet pressure was measured with a pressure transducer. Boiled deionized water was drawn from a liquid tank with a pump and a filter was also placed between them. A buffer tank just after the pump was used to stabilize the flow rate. The accurate liquid flow rate was measured by weighing method (i.e., monitoring the increase in the weight of discharging liquid collected in a container over a period of time). After contacting horizontally in the contactor, two-phase mixture flowed downward into a sealed phase separator through a vertical short tube with 4 mm inner diameter. In order to prevent air from diffusing into the separator, unabsorbed CO_2 was guided through a sufficient long capillary before it vented into air. Three thermocouples (K-type) were located in the inlet ports and the separator, respectively, to measure the corresponding temperatures. All experiments were conducted under ambient conditions (0.1 MPa, 20 °C).

The amount of physically absorbed CO_2 was determined by the standard technique of adding the liquid sample from the phase separator into an excess of NaOH solution and titrating with HCl solution. Phenolphthalein and methyl orange were selected as the indicators for the first and second end-points, respectively. As a blank titration, a similar analysis was also done for the inlet water.

The overall mass transfer contributions in the outlet of SMC I, the connecting short tube and the phase separator were investigated using SMC II shown in Fig. 1(b) under the same operational conditions as those for SMC I. The other experimental setup remained the same as that shown in Fig. 2.

2.2.2. *Chemical mass transfer experiments*

The systems used were CO_2 absorption into a buffer solution of 0.3 M $NaHCO_3$ / 0.3 M Na_2CO_3 and a 1 M NaOH solution. In contrast to physical absorption experiments, two-phase mixture from the outlet of SMC I was directly exposed to air and liquid was collected in an open phase separator because there was no risk of CO_2 escape from the alkaline solution into the air. That is, no connecting tube was needed between the contactor and the phase separator. All experiments were conducted at 25 °C under atmospheric pressure.

The amount of chemically absorbed CO_2 was calculated from concentration changes in the outgoing solution, which was monitored by titrating liquid sample from the phase separator with HCl solution, using phenolphthalein and methyl orange as the indicators for the first and second end-points, respectively.

To account for end effects concerning chemical mass transfer contributions in the outlet of SMC I, reference experiments were also carried out using SMC II shown in Fig. 1(b).

2.2.3. *Two-phase flow pattern visualization*

In order to exhibit mass transfer characteristics in the microchannel clearly, gas–liquid flow patterns under the experimental conditions were also recorded with the aid of a high-speed CCD camera. A cold lamp was used to provide the background illumination for the microchannel. The captured frames were immediately transferred to a personal computer via a data acquisition system for later analysis.

3. Results and discussion

3.1. *Two-phase flow patterns*

The images of two-phase flow encountered during physical mass transfer experiments were analyzed and some typical photographs are demonstrated in Fig. 3. The superficial gas velocity j_G was calculated using the gas density under the local pressure in the observation window by assuming a linear pressure distribution along the microchannel. While for pressure drop and mass transfer data shown in the following sections, j_G was derived based on the average pressure between the microchannel inlet and outlet.

Under the present experimental conditions, stable slug flow was observed at the lowest j_G (Fig. 3(a)). The increase of j_G at the same j_L led to longer bubbles and shorter liquid slugs. At certain j_G, slug flow became unstable, that is, the bubbles approached each other and the length of liquid slugs could not remain constant (Fig. 3(b)). The extremely longer bubble sometimes broke into several parts (Fig. 3(c)).

When j_L was relatively low, increasing j_G led to the merging of the bubbles in slug flow pattern and the slug-annular flow pattern appeared eventually (Fig. 3(d)). This flow pattern resembles an essentially wavy-annular flow if it is not periodically interrupted by large-amplitude solitary waves which do not grow sufficiently to block the flow path (Triplett et al., 1999a).

Churn flow was observed when both j_L and j_G were higher. Similar to the findings of Chung and Kawaji (2004) for N_2-water flow through 250 and 530 μm diameter microchannels, it was also observed that there were two types of churn flow in the present microchannel, i.e., either showing streaks and swirls that trail the gas slug (Fig. 3(e)) or interfacial structures resembling a serpentine-like gas core moving through the liquid (Fig. 3(f)).

Fig. 4 presents the developed flow pattern map for CO_2-water flow in the present microchannel. Many authors have found that the flow patterns in microchannels cannot be satisfactorily described by the widely used flow regime transition models for large channels and therefore new flow pattern maps using superficial velocities as coordinates were proposed (Kawahara et al., 2002; Triplett et al., 1999a; Zhao and Bi, 2001a). Later, Akbar et al. (2003) assessed the available experimental data that dealt with flow regimes of air–water like fluid pairs in near-circular microchannels and devised a flow pattern map using Weber numbers as coordinates. In Figs. 4(a) and (b), the flow transition lines obtained by Triplett et al. (1999a) for a 1.097 mm diameter circular microchannel and those by Akbar et al. (2003) are also included for comparison. It can be seen that the current experimental data are generally in good agreement with the predictions of these two maps. However, it should be noted that the measured transition boundary from slug flow to churn flow in the present microchannel at the highest superficial liquid velocity disagrees with the predictions of the flow pattern map of Akbar et al. (2003). This deviation is partly because of the inconsistent terminology used by these authors for some flow patterns. For example, the flow pattern referred to as churn

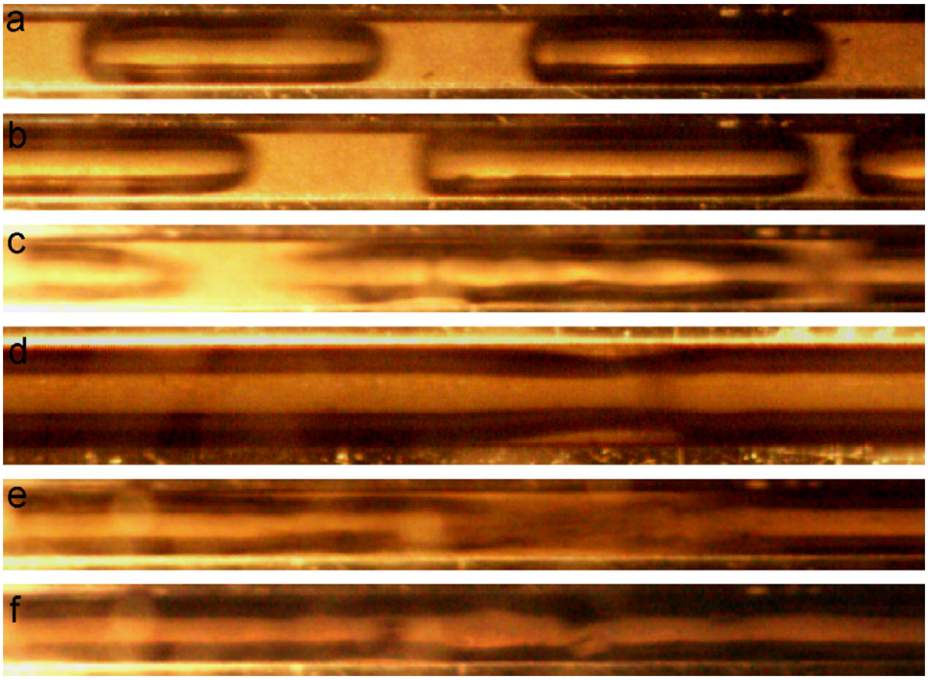

Fig. 3. Representative photographs of CO_2-water flow pattern in the microchannel. Pictures were captured at a distance of 3 cm from the entrance: (a) slug flow ($j_G = 0.73\,\mathrm{m/s},\ j_L = 0.50\,\mathrm{m/s}$); (b) slug flow ($j_G = 0.92\,\mathrm{m/s},\ j_L = 0.50\,\mathrm{m/s}$); (c) slug flow ($j_G = 2.14\,\mathrm{m/s},\ j_L = 1.0\,\mathrm{m/s}$); (d) slug-annular flow ($j_G = 12.7\,\mathrm{m/s},\ j_L = 0.14\,\mathrm{m/s}$); (e) churn flow ($j_G = 9.29\,\mathrm{m/s},\ j_L = 1.0\,\mathrm{m/s}$); (f) churn flow ($j_G = 5.27\,\mathrm{m/s},\ j_L = 1.0\,\mathrm{m/s}$).

flow by Triplett et al. (1999a) is actually subdivided into two different regimes according to the flow pattern map of Akbar et al. (2003): dispersed flow and a flow pattern included in the transition zone. Consequently, the slug-churn transition line of Triplett et al. (1999a) was not considered in the latter paper. Thus more systematic experimental studies are still needed before we can obtain a universal flow pattern map based on dimensionless groups for microchannels.

3.2. Pressure drop

For both physical and chemical mass transfer experiments, the two-phase total pressure drop through the microchannel can be roughly measured as

$$\Delta P_T = P_{\mathrm{in}} - P'_{\mathrm{in}}. \tag{1}$$

Therefore, the frictional two-phase pressure drop for cocurrent gas–liquid flow in the horizontal microchannel can be derived as

$$\Delta P_F = \Delta P_T - \Delta P_A, \tag{2}$$

where

$$\Delta P_A = G^2\left[\left(\frac{x^2}{\rho_G\alpha}+\frac{(1-x)^2}{(1-\alpha)\rho_L}\right)_1-\left(\frac{x^2}{\rho_G\alpha}+\frac{(1-x)^2}{(1-\alpha)\rho_L}\right)_0\right]. \tag{3}$$

The void fraction data in Eq. (3) are evaluated using the Armand correlation, that is,

$$\alpha = 0.833\beta. \tag{4}$$

Eq. (4) was found to be in reasonable agreement with the experimental data of slug flow in microchannels (Serizawa et al., 2002; Zhao and Bi, 2001b).

The acceleration pressure drop thus obtained was found to be negligible compared with the two-phase total pressure drop, ranging from 0.01% to 1.26% of the latter for physical mass transfer experiments. Fig. 5 displays the two-phase frictional pressure drop data as a function of j_L and j_G for CO_2-water flow in the microchannel. Obviously, the two-phase frictional pressure drop increases with the increasing j_L and j_G, which was also observed by many authors (Kawahara et al., 2002; Triplett et al., 1999b; Yue et al., 2004; Zhao and Bi, 2001b).

To predict the two-phase frictional pressure drop data in the microchannel, Lockhart–Martinelli method was used. In this method, the two-phase frictional pressure drop gradient $(\Delta P_F/L)_{TP}$ is correlated with the two-phase friction multiplier Φ_L^2 and the Martinelli parameter X (Lockhart and Martinelli, 1949), that is,

$$\left(\frac{\Delta P_F}{L}\right)_{TP} = \Phi_L^2\left(\frac{\Delta P_F}{L}\right)_L, \tag{5}$$

$$X^2 = \frac{(\Delta P_F/L)_L}{(\Delta P_F/L)_G}, \tag{6}$$

where $(\Delta P_F/L)_L$ and $(\Delta P_F/L)_G$ are the frictional pressure drop gradients when liquid and gas are assumed to flow in the microchannel alone, respectively. The relationship between Φ_L^2 and X can be found from the following widely used Chisholm's

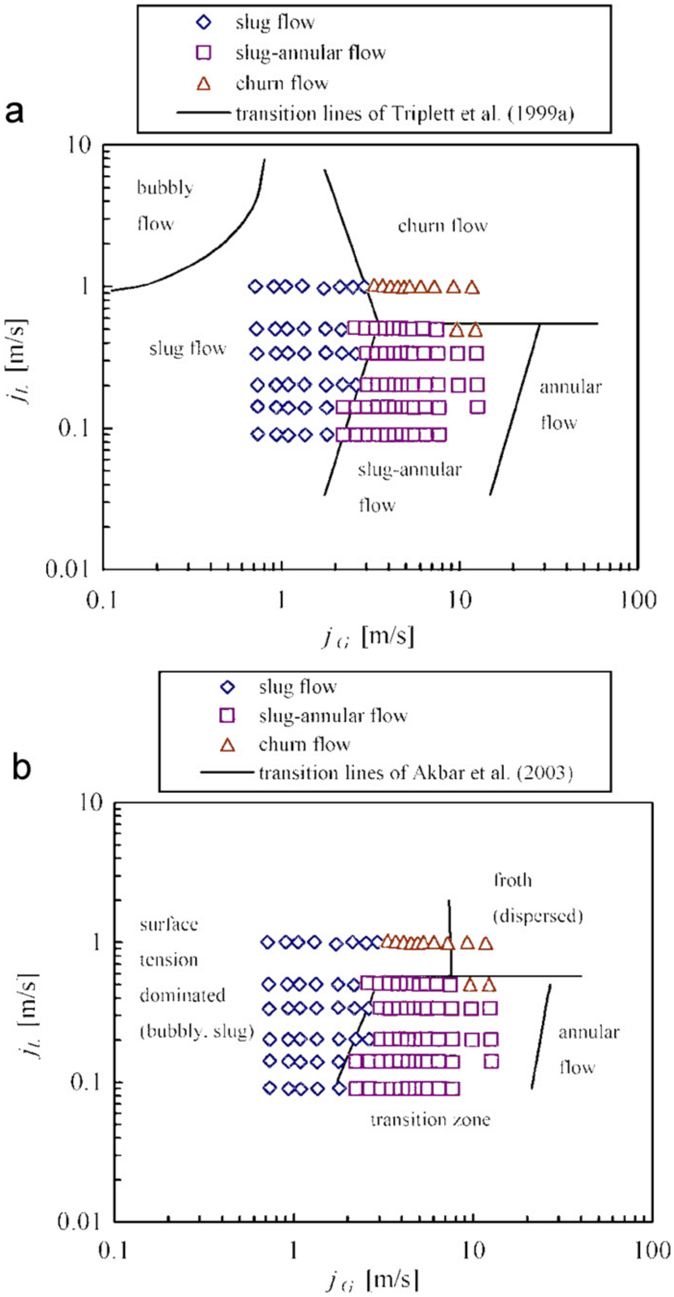

Fig. 4. Comparison of the observed flow pattern data for CO_2-water flow in the microchannel with the flow pattern map of: (a) Triplett et al. (1999a) for a 1.097 mm diameter circular microchannel; (b) Akbar et al. (2003).

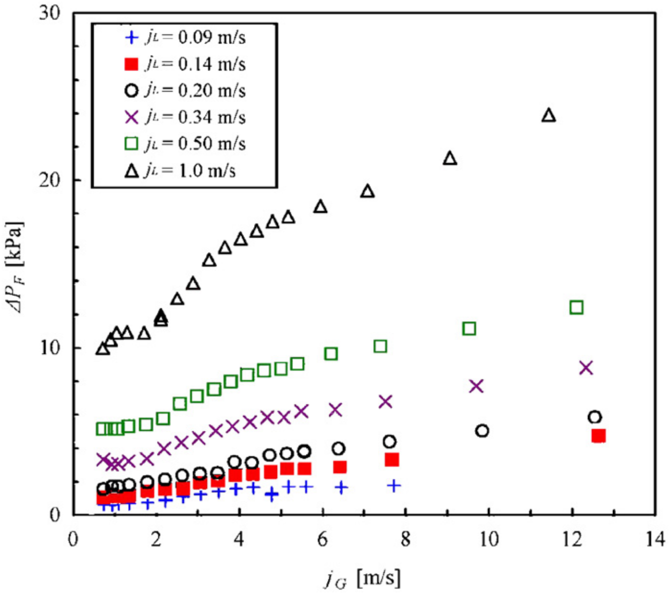

Fig. 5. Measured two-phase frictional pressure drop of CO_2-water flow in the microchannel.

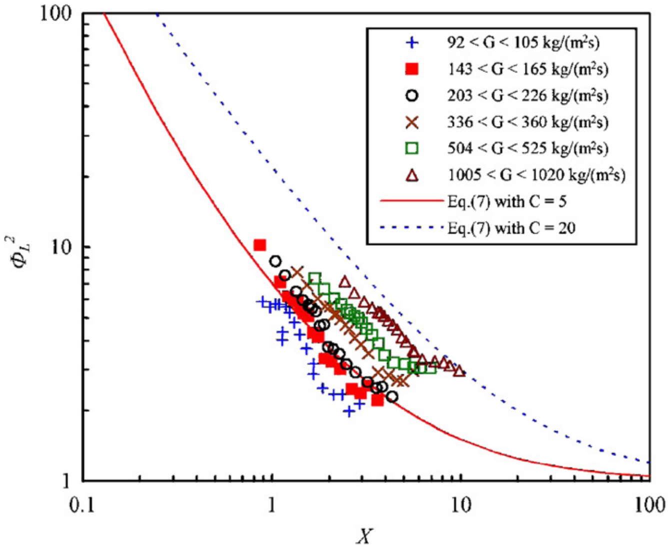

Fig. 6. Measured two-phase frictional multiplier as a function of the Martinelli parameter for physical mass transfer experiments.

equation (Chisholm, 1967):

$$\Phi_L^2 = 1 + \frac{C}{X} + \frac{1}{X^2}, \tag{7}$$

where C is a constant ranging from 5 to 20 dependent on the flow status of gas and liquid in the channel.

Fig. 6 plots the measured two-phase friction multiplier as a function of the Martinelli parameter for physical mass transfer experiments. Because most of the present experiments were conducted under the conditions that both Re_L and Re_G were lower than 1000, C value should be 5 (Chisholm, 1967). However, as can be seen from the figure, the measured two-phase friction multiplier cannot be predicted well by Eq. (7) with a single value of C. Moreover, the experimentally derived C value increases dramatically when there is an increase in the range of mass flux G, showing significant mass flux effect. This effect was first observed in minichannels with $d_h \geqslant 1$ mm (Ali et al., 1993; Wambsganss et al.,1992; Wang et al., 1997). Then the prevalence of such effect in microchannels was found to be also evident. Zhao and Bi (2001b) pointed out that the measured two-phase friction multiplier data for three miniature triangular channels with $d_h = 0.866$, 1.443 and 2.866 mm largely fell between the curves predicted by Eq. (7)

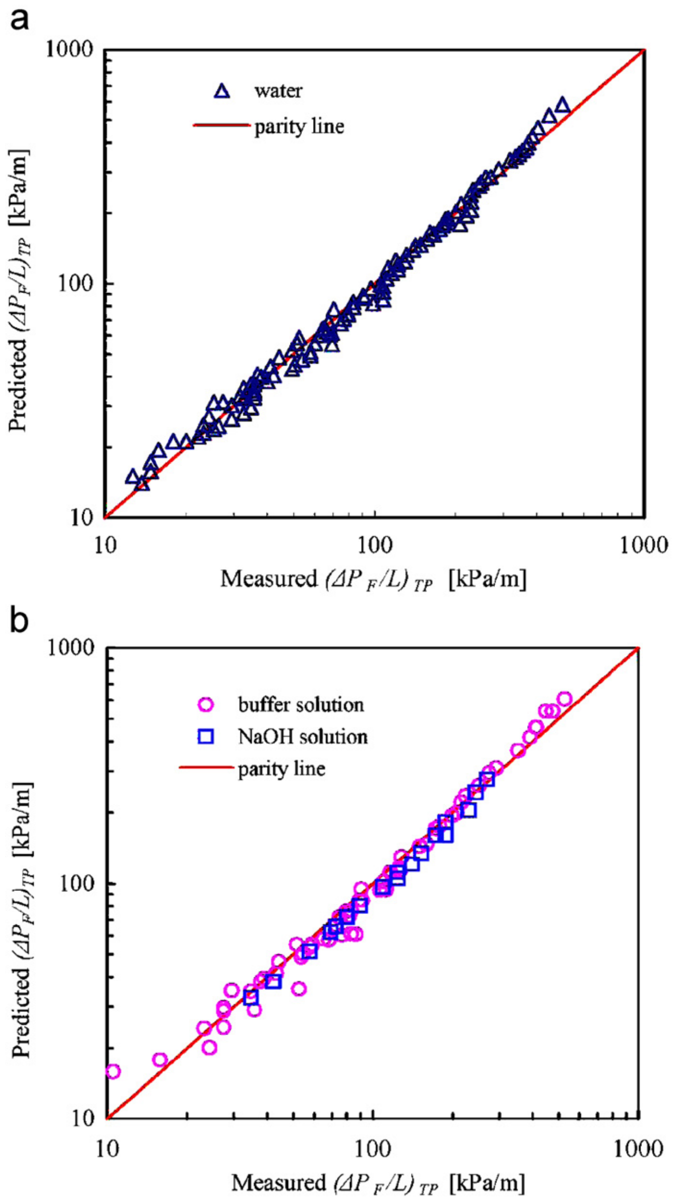

Fig. 7. Comparison between the measured two-phase frictional pressure drop gradient in the microchannel and that predicted by combining Eqs. (5)–(8) for: (a) physical mass transfer experiments; (b) chemical mass transfer experiments.

for $C = 5$ and 20, except the case at very lower superficial liquid velocities. However, what they neglected is that in fact there is a strong evidence of mass flux effect according to their data, especially for the microchannel with $d_h = 0.866$ mm (see Fig. 7(a) in their paper). Yue et al. (2004) noticed this effect in two rectangular microchannels with $d_h = 528$ and 333 μm and then proposed a correlation of C value which could describe their experimental data well. Recently Chung and Kawaji (2004) also proved this effect in N_2-water flow through circular microchannels of 530 and 250 μm diameter. But no correlation accounting for such effect was given in their paper.

Therefore, a similar analysis to that of Yue et al. (2004) was performed based on a least square regression of the obtained C values for physical mass transfer experiments in the microchannel and the following correlation was developed:

$$C = 0.185 X^{-0.0942} Re_{LO}^{0.711}. \tag{8}$$

The predictions of $(\Delta P_F/L)_{TP}$ during CO_2-water flow in the microchannel by combining Eqs. (5) to (8) were found to be in reasonable agreement with the experimental results, as shown in Fig. 7(a), where the standard deviation is as low as 9.2%. To further check the validity of Eq. (8), the measured $(\Delta P_F/L)_{TP}$ data in chemical mass transfer experiments are also compared with the model predictions (Fig. 7(b)). The standard deviations in this case are only 13.3% and 10.2% for the buffer solution and NaOH solution, respectively. Thus Lockhart–Martinelli method is still applicable to represent two-phase frictional pressure drop characteristics in the present microchannel if the proposed correlation of C value in the Chisholm's equation is employed.

3.3. *Mass transfer characteristics*

3.3.1. *Liquid side volumetric mass transfer coefficient in the microchannel measured by physical absorption method*

For physical absorption of CO_2 into water, liquid side volumetric mass transfer coefficient $k_L a$ in the present microchannel can be represented as

$$k_L a = \frac{j_L}{L} \ln\left(\frac{C^* - C_{CO_2,0}}{C^* - C_{CO_2,1}}\right). \tag{9}$$

End effects were eliminated by taking two sets of experiments using SMC I and SMC II shown in Figs. 1(a) and (b), respectively. Therefore, $k_L a$ can be measured from the experiments as (Yue et al., 2006)

$$k_L a = \frac{j_L}{L} \ln\left(\frac{C^* - C_{CO_2,3}}{C^* - C_{CO_2,2}}\right). \tag{10}$$

Fig. 8 depicts the measured $k_L a$ in the microchannel as a function of j_L and j_G. The experimentally observed flow pattern transition boundary between slug flow and slug-annular flow or churn flow for each j_L is also plotted in this figure. It is shown that when the microchannel is operated under these flow patterns, $k_L a$ value increases significantly with the increasing j_L and j_G, which is similar to mass transfer behavior generally observed in minichannels with $d_h \geqslant 1$ mm (Luo and Ghiaasiaan, 1997; Tortopidis and Bontozoglou, 1997; Vandu et al., 2005).

It is commonly accepted that liquid side volumetric mass transfer coefficients in large pipes can be well correlated with the energy dissipation parameter ε (Jagota et al., 1973; Jepsen, 1970; Tortopidis and Bontozoglou, 1997), defined as

$$\varepsilon = \left(\frac{\Delta P_F}{L}\right)_{TP} (j_G + j_L). \tag{11}$$

However, it was found (Yue et al., 2006) that the measured $k_L a$ value in the present microchannel can be better predicted using $(\Delta P_F/L)_{TP}$ instead of ε as the fitting parameter, where the

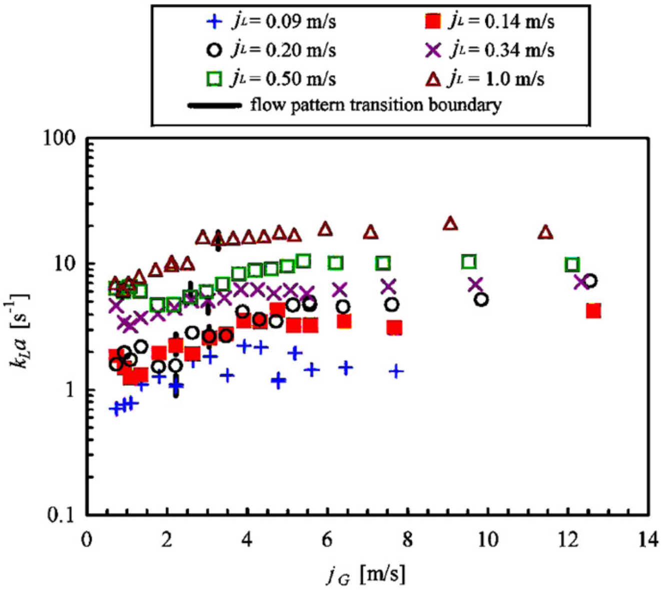

Fig. 8. Effect of superficial gas and liquid velocities on liquid side volumetric mass transfer coefficient in the microchannel measured by physical absorption method.

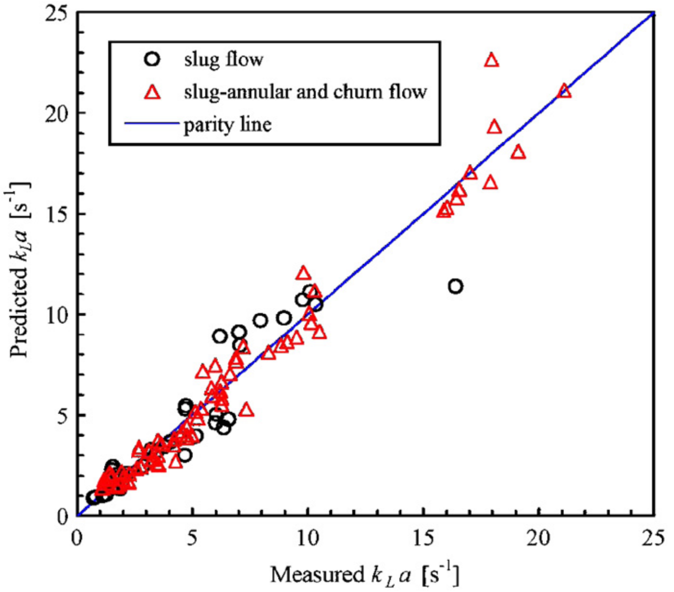

Fig. 9. Comparison between liquid side volumetric mass transfer coefficient in the microchannel measured by physical absorption method and that predicted by Eqs. (13) and (14).

standard deviation is only 18.9% in the former case, in contrast to 45.9% in the latter case. That is, the following correlation was obtained:

$$k_La = 0.0863\left(\frac{\Delta P_F}{L}\right)_{TP}^{0.881}. \tag{12}$$

Another more justified method to correlate liquid side volumetric mass transfer coefficient is to use dimensionless empirical correlations (Luo and Ghiaasiaan, 1997; Scott and Hayduk, 1966; Shilimkan and Stepanek, 1977b). Through a least square regression of the experimental data, separate correlations were developed for different flow patterns in order to display physical mass transfer characteristics in the present microchannel. That is, for slug flow:

$$Sh_L \cdot a \cdot d_h = 0.084\ Re_G^{0.213} Re_L^{0.937} Sc_L^{0.5} \tag{13}$$

and for slug-annular flow and churn flow:

$$Sh_L \cdot a \cdot d_h = 0.058 Re_G^{0.344} Re_L^{0.912} Sc_L^{0.5}. \tag{14}$$

Fig. 9 shows the good predicting performance of Eqs. (13) and (14) with standard deviations of 22.8% and 19%, respectively.

3.3.2. Liquid side volumetric mass transfer coefficient in the microchannel measured by chemical absorption method

Due to very high mass transfer rate, a certain gas–liquid system in the microchannel may fall into different reaction regime from those in conventional-sized vessels depending on the relative rates of diffusion and reaction (Danckwerts, 1970). Consequently, the applicability of currently available gas–liquid systems for investigation of mass transfer parameters to microchannel contactors should be carefully checked.

In the present investigation, the absorption of CO_2 into a buffer solution of 0.3 M $NaHCO_3$ / 0.3 M Na_2CO_3 was chosen to characterize liquid side volumetric mass transfer coefficient in the microchannel. The global reaction that occurs is (Danckwerts, 1970)

$$CO_2 + CO_3^{2-} + H_2O \rightarrow 2HCO_3^-. \tag{15}$$

According to the experimental results of Roberts and Danckwerts (1962), the apparent first-order rate constant for this reaction, $k_{1,\mathrm{app}} = 0.86\,\mathrm{s}^{-1}$. From Fig. 8 we can see that k_La value for physical absorption experiments in the present microchannel ranges from 0.7 to 21 s^{-1}. Therefore, it is anticipated that when CO_2 is absorbed into the buffer solution in the microchannel under the same ranges of j_L and j_G as those for physical absorption experiments, the following inequality should be fulfilled,

$$k_La \gg (1-\alpha)k_{1,\mathrm{app}}. \tag{16}$$

It means that in the present microchannel the reaction rate is very much slower than the transfer rate of CO_2 into the solution, thus the absorption process can be treated as a physical one and CO_2 absorbed remains unreacted in the bulk liquid. Under this condition, the specific rate of absorption in the microchannel can be written as

$$R_{mc} = k_L(C^* - C_{CO_2}). \tag{17}$$

A mass balance for dissolved CO_2 in the bulk liquid over an elementary volume of the microchannel will result in

$$-Q_L\,\mathrm{d}C_{CO_2} = k_La(C^* - C_{CO_2})\,\mathrm{d}V_{mc}. \tag{18}$$

By assuming that k_La is constant and integrating Eq. (18) over the entire microchannel volume, k_La in the microchannel can be derived as

$$k_La = \frac{Q_L}{V_{mc}} \ln\left(\frac{C^* - C_{CO_2,0}}{C^* - C_{CO_2,1}}\right), \tag{19}$$

where $C_{CO_2,0} = 0$.

When two-phase mixture left from the microchannel to the outlet region of SMC I, there was still large gas–liquid contacting. As the outlet region is more like a tube of 6 mm diameter (Fig. 1(a)), liquid side volumetric mass transfer coefficient here is thought to be very low under the present experimental conditions and the following inequalities are satisfied (Kasturi and Stepanek, 1974b; Shilimkan and Stepanek, 1977b; Tortopidis and Bontozoglou, 1997),

$$(k_La)_{out} \ll (1-\alpha)k_{1,app}, \tag{20}$$

$$k^2_{L,out} \gg D_{CO_2}k_{1,app}. \tag{21}$$

In this case, the rate of reaction in the diffusion film is negligible and the concentration of CO_2 in the bulk liquid is nearly zero. Then the absorption rate of CO_2 in the outlet region is (Danckwerts, 1970)

$$R_{out} = k_{L,out}C^*. \tag{22}$$

Therefore, a mass balance for $C_{CO_3^{2-}}$ over an elementary volume of the outlet region can be written as

$$-Q_L\, dC_{CO_3^{2-}} = (k_La)_{out}C^*\, dV_{out} \tag{23}$$

And by integrating we can derive the average liquid side volumetric mass transfer coefficient in the outlet region as

$$(k_La)_{out} = \frac{Q_L(C_{CO_3^{2-},0} - C_{CO_2,1} - C_{CO_3^{2-},2})}{C^*V_{out}}. \tag{24}$$

Also in the reference experiment using SMC II shown in Fig. 1(b) under the same experimental conditions, there should be

$$(k_La)_{out} = \frac{Q_L(C_{CO_3^{2-},0} - C_{CO_3^{2-},3})}{C^*V_{out}}. \tag{25}$$

Therefore we have

$$C_{CO_2,1} = C_{CO_3^{2-},3} - C_{CO_3^{2-},2}. \tag{26}$$

From Eqs. (19) and (26), k_La value in the microchannel can be calculated as

$$k_La = \frac{j_L}{L}\left(\frac{C^*}{C^* + C_{CO_3^{2-},2} - C_{CO_3^{2-},3}}\right). \tag{27}$$

Fig. 10 demonstrates the evolution of the measured k_La value in the microchannel versus j_L and j_G. The same tendency as that shown in Fig. 8 is observed, i.e., k_La value increases with an increase in j_L or j_G. However, the obtained k_La value by the present chemical method is generally lower than that measured by physical absorption method at the same j_L and j_G, which is thought to result from a lower diffusivity of CO_2 in the buffer solution than that in water.

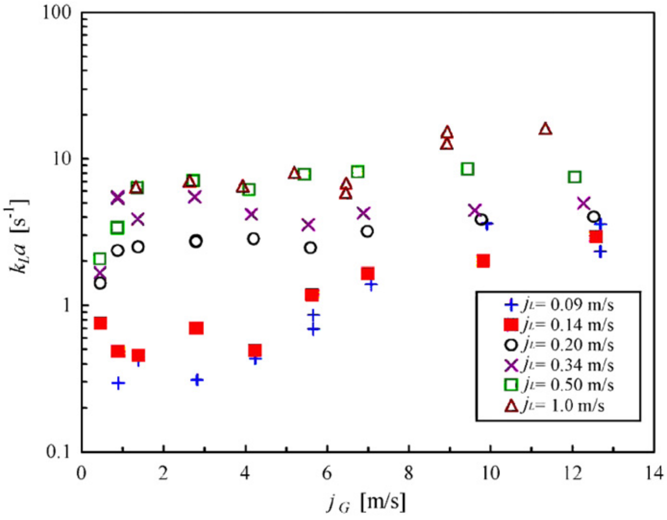

Fig. 10. Effect of superficial gas and liquid velocities on liquid side volumetric mass transfer coefficient in the microchannel measured by chemical absorption method.

3.3.3. Interfacial area in the microchannel measured by the chemical method

The chemical method based on the absorption of CO_2 into a 1 M NaOH solution was applied to determine interfacial area in the microchannel. The reactions occurring can be expressed as

$$CO_2 + OH^- \rightarrow HCO_3^-, \tag{28}$$

$$HCO_3^- + OH^- \rightarrow CO_3^{2-} + H_2O. \tag{29}$$

The reaction (28) is rate controlling due to its significantly lower reaction rate than that of reaction (29). A general correlation of the second-order rate constant for reaction (28), k_{OH^-}, was suggested by Pohorecki and Moniuk (1988):

$$\log_{10} k_{OH^-} = 11.916 - \frac{2382}{T} + \sum b_{ion}I_{ion}. \tag{30}$$

Reaction (28) can be regarded as a fast and pseudo-first-order reaction in the present microchannel under certain experimental conditions, provided the following criteria are satisfied (Danckwerts, 1970),

$$\sqrt{\frac{D_{CO_2}k_{OH^-}C_{OH^-}}{k_L^2}} \ll \sqrt{\frac{D_{CO_2}}{D_{OH^-}}} + \frac{C_{OH^-}}{2C^*}\sqrt{\frac{D_{OH^-}}{D_{CO_2}}}, \tag{31}$$

$$\sqrt{\frac{D_{CO_2}k_{OH^-}C_{OH^-}}{k_L^2}} \gg 3. \tag{32}$$

That is, CO_2 is entirely consumed in the diffusion film and the interfacial concentration of OH^- is practically the same as that in the bulk liquid phase. Recently Zanfir et al. (2005) have tested this absorption process in a falling film microreactor containing 64 microchannels of 300 × 100 µm and found that CO_2 was completely reacted within a very short distance from the gas–liquid interface and the concentration of OH^- did not decrease to zero near the interface, indicating that the limiting step for this reaction occuring in their microreactor is still CO_2 mass transfer in the liquid phase.

In this case, the specific rate of absorption is given by

$$R = C^* \sqrt{D_{CO_2} k_{OH^-} C_{OH^-}}. \tag{33}$$

Therefore, similar to the deduction put in Section 3.3.2, interfacial area in the microchannel is derived as

$$a = \frac{Q_L\left(\sqrt{C_{OH^-,0}} - \sqrt{C_{OH^-,1}}\right)}{C^* V_{mc}\sqrt{D_{CO_2} k_{OH^-}}}. \tag{34}$$

As to the mass transfer contributions in the outlet region of SMC I, it is thought that reaction (28) can be considered as instantaneous due to much lower liquid side mass transfer coefficient there (Kasturi and Stepanek, 1974b; Shilimkan and Stepanek, 1977b). In other words, the following criterion is fulfilled (Danckwerts, 1970):

$$\sqrt{\frac{D_{CO_2} k_{OH^-} C_{OH^-}}{k_{L,\mathrm{out}}^2}} \gg \sqrt{\frac{D_{CO_2}}{D_{OH^-}}} + \frac{C_{OH^-}}{2C^*}\sqrt{\frac{D_{OH^-}}{D_{CO_2}}}. \tag{35}$$

And under the present experimental conditions, the following inequality exists

$$\frac{C_{OH^-} D_{OH^-}}{2C^* D_{CO_2}} \gg 1. \tag{36}$$

In this case, the specific rate of absorption is

$$R_{\mathrm{out}} = \frac{k_{L,\mathrm{out}} C_{OH^-}}{2}\sqrt{\frac{D_{OH^-}}{D_{CO_2}}}. \tag{37}$$

Therefore, we can deduce the average liquid side volumetric mass transfer coefficient in the outlet region as

$$(k_L a)_{\mathrm{out}} = \frac{Q_L}{V_{\mathrm{out}}}\sqrt{\frac{D_{OH^-}}{D_{CO_2}}}\ln\left(\frac{C_{OH^-,1}}{C_{OH^-,2}}\right). \tag{38}$$

In the reference experiment using SMC II shown in Fig. 1 (b), we can also get

$$(k_L a)_{\mathrm{out}} = \frac{Q_L}{V_{\mathrm{out}}}\sqrt{\frac{D_{OH^-}}{D_{CO_2}}}\ln\left(\frac{C_{OH^-,0}}{C_{OH^-,3}}\right). \tag{39}$$

From Eqs. (38) and (39) it is obtained that

$$C_{OH^-,1} = \frac{C_{OH^-,0} C_{OH^-,2}}{C_{OH^-,3}}. \tag{40}$$

Thus interfacial area in the microchannel can be measured as

$$a = \frac{j_L}{C^* L\sqrt{D_{CO_2} k_{OH^-}}}\left(\sqrt{C_{OH^-,0}} - \sqrt{\frac{C_{OH^-,0} C_{OH^-,2}}{C_{OH^-,3}}}\right). \tag{41}$$

The measured a values in the microchannel are reported in Fig. 11. As can be seen, a generally increases with increasing j_G, especially at lower j_L. However, the effect of j_L on a is not very marked. Under the operational conditions listed in this figure, slug flow was observed at lower j_G while slug-annular flow dominated at higher j_G. Therefore, an increase in j_G at a fixed j_L in slug flow pattern will cause longer bubbles and shorter liquid slugs, which will contribute to a larger interfacial area. In slug-annular flow pattern, the evolution of interfacial area with j_G will be somewhat complicated due to the irregular motion of gas–liquid interface. In large tube reactors, many authors have found that interfacial areas were strongly affected by such parameters as liquid holdup and gas–liquid flow structure (Kasturi and Stepanek, 1974a; Shilimkan and Stepanek, 1977a, 1978; Tomida et al., 1978). Therefore, a more detailed inspection of gas–liquid flow in the microchannel under real reaction conditions should be more helpful to elucidate this phenomenon.

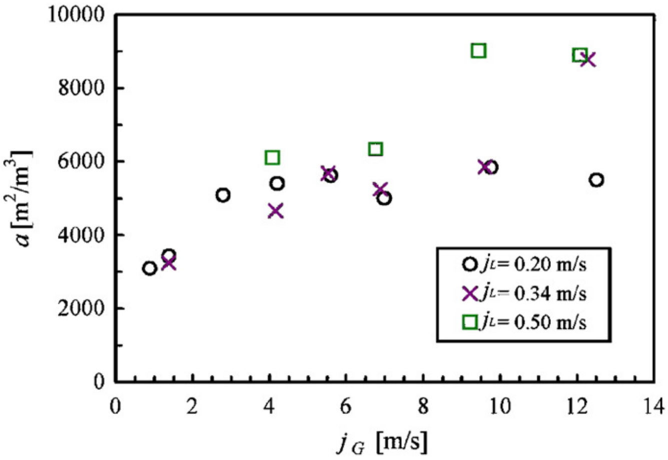

Fig. 11. Effect of superficial gas and liquid velocities on interfacial area in the microchannel measured by the chemical method.

3.3.4. *Deduction of liquid side mass transfer coefficient in the microchannel*

Since the density and viscosity of a 1 M NaOH solution are almost equal to those of a 0.3 M $NaHCO_3$ / 0.3 M Na_2CO_3 buffer solution, two-phase flow characteristics met during CO_2 absorption into these solutions in the microchannel are thought to be similar under the same experimental conditions, which has already been evidenced by the measured pressure drop and flow pattern data. Due to nearly equal CO_2 diffusivity in both solutions, the corresponding liquid side volumetric mass transfer coefficients would be nearly equal too. Hence, liquid side mass transfer coefficient, k_L in the microchannel can be evaluated based on dividing the $k_L a$ value previously determined for CO_2-buffer solution system by the measured a for CO_2–NaOH solution system at the same flow rates of gas and liquid. Fig. 12 summarizes the derived k_L in the microchannel. On the whole k_L shows a remarkable increase with j_L at a fixed j_G. However, the influence of j_G on k_L is insignificant.

With the data presented in Fig. 12, the necessary criteria for the determination of interfacial area in the microchannel can now be examined. As shown in Table 1, inequalities (31) and (32) are thought to be valid everywhere along the microchannel under the present operational conditions. Therefore, the chosen chemical method is reliable for the determination of interfacial areas in the microchannel without much experimental error (Danckwerts, 1970).

From the curves shown in Fig. 8, Figs. 10–12, it can be concluded that for a given j_L, the increase of $k_L a$ with j_G in the microchannel is largely due to an increase in a while for a given j_G, the increase of $k_L a$ with j_L is mainly a result of a significant increase in k_L.

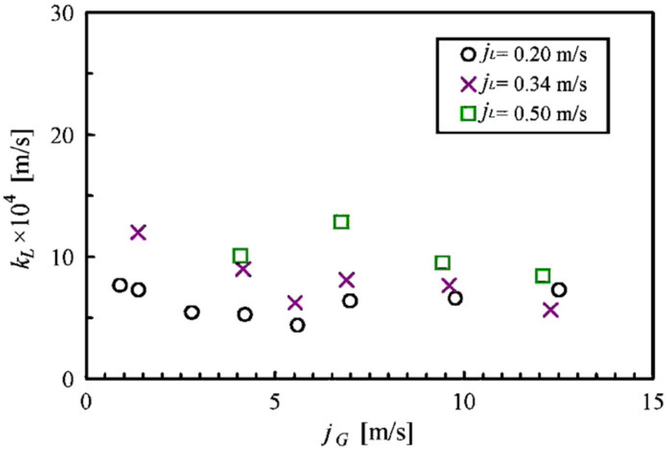

Fig. 12. Effect of superficial gas and liquid velocities on liquid side mass transfer coefficient in the microchannel measured by the chemical method.

3.4. *Comparison of mass transfer performance among different gas–liquid contactors*

Table 2 lists typical mass transfer parameters measured in the microchannel (Fig. 8, Figs. 10–12), as well as those for some gas–liquid contactors frequently used in laboratories and industries. It is demonstrated from this table that liquid side volumetric mass transfer coefficient and interfacial area in the microchannel structure are at least one or two orders of magnitude higher than those in traditional contactors such as bubble columns, packed columns. When the microchannel size is further reduced, much higher interfacial area is expected (Haverkamp et al., 2002; Jähnisch et al., 2000). For example, Haverkamp et al. (2002) measured gas–liquid interfacial areas in a 300 μm wide, 100 μm deep microchannel using optical method and found that the maximum value could reach $18,000\,\mathrm{m}^2/\mathrm{m}^3$, which is very difficult to achieve in conventional devices. Therefore, significant mass transfer intensification in the microchannel implies that the adoption of gas–liquid microchemical systems is very beneficial to many industrially important gas–liquid mass transfer operations and reactions.

4. Conclusions

In this study, gas–liquid flow and mass transfer characteristics in a rectangular microchannel with a hydraulic diameter of 667 μm have been investigated by the absorption of CO_2 into

Table 1
Verification of necessary criteria for interfacial area measurements in the microchannel under some typical experimental conditions (Ref.: inequalities (31) and (32))

j_G (m/s)	j_L (m/s)	$\sqrt{\frac{D_{CO_2} k_{OH^-} C_{OH^-}}{k_L^2}}$		$\sqrt{\frac{D_{CO_2}}{D_{OH^-}}} + \frac{C_{OH^-}}{2C^*}\sqrt{\frac{D_{OH^-}}{D_{CO_2}}}$		a (m^2/m^3)
		Microchannel inlet	Microchannel outlet	Microchannel inlet	Microchannel outlet	
1.38	0.20	6.13	5.59	26.98	22.51	3429
12.5	0.20	6.15	5.25	26.57	19.58	5511
1.37	0.34	3.73	3.54	26.77	24.16	3251
12.3	0.34	7.92	6.79	26.10	19.39	8786
4.08	0.50	4.45	4.15	26.12	22.87	6101
12.1	0.50	5.30	4.78	25.60	20.97	8899

Table 2
Comparison of mass transfer parameters in different gas–liquid contactors

Type of contactor	$k_L \times 10^5$ (m/s)	a (m^2/m^3)	$k_L a \times 10^2$ (s^{-1})
Bubble columns (Charpentier, 1981)	10–40	50–600	0.5–24
Couette–Taylor flow reactor (Dlusa et al., 2004)	9–20	200–1200	3–21
Impinging jet absorbers (Herskowits et al., 1990)	29–66	90–2050	2.5–122
Packed columns, cocurrent (Charpentier, 1981)	4–60	10–1700	0.04–102
Packed columns, countercurrent (Charpentier, 1981)	4–20	10–350	0.04–7
Spray column (Kies et al., 2004)	12–19	75–170	1.5–2.2
Static mixers (Heyouni et al., 2002)	100–450	100–1000	10–250
Stirred tank (Kies et al., 2004)	0.3–80	100–2000	3–40
Tube reactors, horizontal and coiled (Charpentier, 1981)	10–100	50–700	0.5–70
Tube reactors, vertical (Charpentier, 1981)	20–50	100–2000	2–100
Gas–liquid microchannel contactor of this study	40–160	3400–9000	30–2100

water, a 0.3 M $NaHCO_3$ / 0.3 M Na_2CO_3 buffer solution and a 1 M NaOH solution. The ranges of superficial gas and liquid velocities were 0.7–13 m/s and 0.09–1.0 m/s, respectively. The following conclusions can be drawn from the results of this paper:

(1) For CO_2-water flow through the microchannel, slug flow, slug-annular flow and churn flow were observed. The experimental data are in overall good agreements with the predictions of the flow pattern maps proposed by Triplett et al. (1999a) and Akbar et al. (2003).
(2) For both physical and chemical mass transfer experiments, the two-phase frictional pressure drop in the microchannel can be well predicted by Lockhart–Martinelli method if the proposed new correlation of C value in the Chisholm's equation accounting for mass flux effect is employed.
(3) At a fixed superficial liquid velocity, both liquid side volumetric mass transfer coefficient and interfacial area in the microchannel increase with an increase in superficial gas velocity, while the change of liquid side mass transfer coefficient is insignificant. At a fixed superficial gas velocity, both liquid side volumetric mass transfer coefficient and liquid side mass transfer coefficient in the microchannel show dramatic increases with an increase in superficial liquid velocity, while the effect of superficial liquid velocity on interfacial area is not very marked.
(4) The developed empirical correlations (Eqs. (12)–(14)) can predict the measured liquid side volumetric mass transfer coefficient in the microchannel for CO_2-water system with standard deviations less than 23%.
(5) Liquid side volumetric mass transfer coefficient and interfacial area in the present microchannel are measured to be as high as 21 s^{-1} and 9000 m^2/m^3, respectively, which are at least one or two orders of magnitude higher than those in conventional gas–liquid contactors, thus showing the great potential of gas–liquid microchemical systems for many industrially relevant gas–liquid mass transfer operations and reactions.

Notation

a	interfacial area, m^2/m^3
b_{ion}	contribution of an ion in Eq. (30), m^3/mol
C	coefficient in the Chisholm's equation, Eq. (7)
C_A	molar concentration of component A in the liquid ($A = CO_2,\ OH^-,\ HCO_3^-,\ CO_3^{2-}$), mol/m^3
C^*	physical solubility of CO_2 in the liquid, mol/m^3
d_h	hydraulic diameter, m
D_{CO_2}	diffusivity of CO_2 in the liquid, m^2/s
D_{OH^-}	effective diffusivity of hydroxyl ion in the liquid, m^2/s
G	mass flux, defined by ($= j_G\rho_G + j_L\rho_L$), $kg/(m^2\,s)$
I_{ion}	contribution of an ion in the ionic strength of solution, mol/m^3
j_G	superficial gas velocity, m/s
j_L	superficial liquid velocity, m/s
$k_{1,app}$	pseudo-first-order rate constant, s^{-1}
k_L	liquid side mass transfer coefficient, m/s
k_La	liquid side volumetric mass transfer coefficient, s^{-1}
k_{OH^-}	rate constant for reaction between carbon dioxide and hydroxyl ion, $m^3/(mol\,s)$
L	length of the microchannel, m
P_{in}	inlet gas pressure in SMC I, Pa
P'_{in}	inlet gas pressure in SMC II , Pa
ΔP_A	two-phase acceleration pressure drop, Pa
ΔP_F	two-phase frictional pressure drop, Pa
ΔP_T	two-phase total pressure drop, Pa
Q	flow rate, m^3/s
R	rate of absorption per unit interfacial area, $mol/(m^2\,s)$
Re_G	superficial gas Reynolds number defined by ($= d_h j_G \rho_G/\mu_G$), dimensionless
Re_L	superficial liquid Reynolds number defined by ($= d_h j_L \rho_L/\mu_L$), dimensionless
Re_{LO}	Reynolds number for liquid flowing at the two-phase mass flux defined by ($= d_h G/\mu_L$), dimensionless
Sc_L	liquid Schmidt number defined by ($= \mu_L/\rho_L D_{CO_2}$), dimensionless
Sh_L	liquid Sherwood number defined by ($= k_L d_h/D_{CO_2}$), dimensionless
T	temperature, K
V	volume, m^3
x	gas mass fraction
X	Martinelli parameter

Greek letters

α	void fraction
β	gas volumetric flow ratio
ε	energy dissipation parameter
μ	viscosity, Pa s
ρ	density, kg/m^3
Φ_L^2	two-phase frictional multiplier

Subscripts

0	microchannel inlet
1	microchannel outlet
2	in the phase separator during experiments with SMC I
3	in the phase separator during reference experiment with SMC II
G	gas phase
L	liquid phase
mc	microchannel
out	the outlet region of SMC I
TP	two-phase mixture

Acknowledgments

The authors wish to gratefully acknowledge the financial supports for this project from National Natural Science Foundation of China (Nos. 20490208 and 20676129), Key Program for International Cooperation of Science and Technology (No. 2001CB711203), and Youth Fund of Dalian Institute of Chemical Physics, Chinese Academy of Sciences (No. S200401).

References

Akbar, M.K., Plummer, D.A., Ghiaasiaan, S.M., 2003. On gas–liquid two-phase flow regimes in microchannels. International Journal of Multiphase Flow 29, 855–865.

Ali, M.I., Sadatomi, M., Kawaji, M., 1993. Adiabatic two-phase flow in narrow channels between two flat plates. Canadian Journal of Chemical Engineering 71, 657–666.

Charpentier, J.C., 1981. Mass-transfer rates in gas–liquid absorbers and reactors. Advances in Chemical Engineering 11, 1–133.

Chisholm, D., 1967. A theoretical basis for the Lockhart–Martinelli correlation for two-phase flow. International Journal of Heat and Mass Transfer 10, 1767–1778.

Chung, P.M.-Y., Kawaji, M., 2004. The effect of channel diameter on adiabatic two-phase flow characteristics in microchannels. International Journal of Multiphase Flow 30, 735–761.

Danckwerts, P.V., 1970. Gas–liquid Reactions. McGraw-Hill, New York.

de Mas, N., Gunther, A., Schmidt, M.A., Jensen, K.F., 2003. Microfabricated multiphase reactors for the selective direct fluorination of aromatics. Industrial & Engineering Chemistry Research 42, 698–710.

Dlusa, E., Wronski, S., Ryszczuk, T., 2004. Interfacial area in gas–liquid Couette–Taylor flow reactor. Experimental Thermal and Fluid Science 28, 467–472.

Ehrfeld, W., Hessel, V., Löwe, H., 2000. Microreactors: New Technology For Modern Chemistry. Wiley-VCH, Weinheim.

Haverkamp, V., Emig, G., Hessel, V., Liauw, M.A., Löwe, H., 2002. Characterization of a gas/liquid microreactor the micro bubble column: determination of specific interfacial area. In: Matlosz, M., Ehrfeld, W., Baselt, J.P. (Eds.), Microreaction Technology: IMRET 5: Proceedings of the Fifth International Conference on Microreaction Technology. Springer, Berlin, Heidelberg, New York, pp. 202–213.

Herskowits, D., Herskowits, V., Stephan, K., Tamir, A., 1990. Characterization of a two-phase impinging jet absorber II. Absorption with chemical reaction of CO_2 in NaOH solutions. Chemical Engineering Science 45, 1281–1287.

Hessel, V., Angeli, P., Gavriilidis, A., Löwe, H., 2005. Gas–liquid and gas–liquid–solid microstructured reactors: contacting principles and applications. Industrial & Engineering and Chemistry Research 44, 9750–9769.

Heyouni, A., Roustan, M., Do-Quang, Z., 2002. Hydrodynamics and mass transfer in gas–liquid flow through static mixers. Chemical Engineering Science 57, 3325–3333.

Jagota, A.K., Rhodes, E., Scott, D.S., 1973. Mass transfer in upwards co-current gas–liquid annular flow. Chemical Engineering Journal 5, 23–31.

Jähnisch, K., Baerns, M., Hessel, V., Ehrfeld, W., Haverkamp, V., Löwe, H., Wille, Ch., Guber, A., 2000. Direct fluorination of toluene using elemental fluorine in gas/liquid microreactors. Journal of Fluorine Chemistry 105, 117–128.

Jähnisch, K., Hessel, V., Löwe, H., Baerns, M., 2004. Chemistry in microstructured reactors. Angewandte Chemie-International Edition 43, 406–446.

Jensen, K.F., 2001. Microreaction engineering—is small better? Chemical Engineering Science 56, 293–303.

Jepsen, J.C., 1970. Mass transfer in two-phase flow in horizontal pipelines. A.I.CH.E. Journal 16, 705–711.

Kasturi, G., Stepanek, J.B., 1974a. Two-phase flow—III. Interfacial area in cocurrent gas–liquid flow. Chemical Engineering Science 29, 713–719.

Kasturi, G., Stepanek, J.B., 1974b. Two-phase flow—IV. Gas and liquid side mass transfer coefficients. Chemical Engineering Science 29, 1849–1856.

Kawahara, A., Chung, P.M.-Y., Kawaji, M., 2002. Investigation of two-phase flow pattern, void fraction and pressure drop in a microchannel. International Journal of Multiphase Flow 28, 1411–1435.

Kies, F.K., Benadda, B., Otterbein, M., 2004. Experimental study on mass transfer of a co-current gas–liquid contactor performing under high gas velocities. Chemical Engineering and Processing 43, 1389–1395.

Kobayashi, J., Mori, Y., Okamoto, K., Akiyama, R., Ueno, M., Kitamori, T., Kobayashi, S., 2004. A microfluidic device for conducting gas–liquid–solid hydrogenation reactions. Science 304, 1305–1308.

Kolb, G., Hessel, V., 2004. Micro-structured reactors for gas phase reactions. Chemical Engineering Journal 98, 1–38.

Löb, P., Löwe, H., Hessel, V., 2004. Fluorinations, chlorinations and brominations of organic compounds in microreactors. Journal of Fluorine Chemistry 125, 1677–1694.

Lockhart, R.W., Martinelli, R.C., 1949. Proposed correlation of data for isothermal two-phase two-component flow in pipes. Chemical Engineering Progress 45, 39–48.

Luo, D., Ghiaasiaan, S.M., 1997. Liquid-side interphase mass transfer in cocurrent vertical two-phase channel flows. International Journal of Heat and Mass Transfer 40, 641–655.

Pohorecki, R., Moniuk, W., 1988. Kinetics of reaction between carbon dioxide and hydroxyl ions in aqueous electrolyte solutions. Chemical Engineering Science 43, 1677–1684.

Roberts, D., Danckwerts, P.V., 1962. Kinetics of CO_2 absorption in alkaline solutions—I. Transient absorption rates and catalysis by arsenite. Chemical Engineering Science 17, 961–969.

Scott, D.S., Hayduk, W., 1966. Gas absorption in horizontal cocurrent bubble flow. Canadian Journal of Chemical Engineering 44, 130–136.

Serizawa, P.A., Feng, Z.P., Kawara, Z., 2002. Two-phase flow in microchannels. Experimental Thermal and Fluid Science 26, 703–714.

Shilimkan, R.V., Stepanek, J.B., 1977a. Interfacial area in cocurrent gas–liquid upward flow in tubes of various size. Chemical Engineering Science 32, 149–154.

Shilimkan, R.V., Stepanek, J.B., 1977b. Effect of tube size on liquid side mass transfer in cocurrent gas–liquid upward flow. Chemical Engineering Science 32, 1397–1400.

Shilimkan, R.V., Stepanek, J.B., 1978. Mass transfer in cocurrent gas–liquid flow: gas side mass transfer coefficients in upflow, interfacial areas and mass transfer coefficient in gas and liquid in downflow. Chemical Engineering Science 33, 1675–1680.

Tegrotenhuis, W.E., Cameron, R.J., Viswanathan, V.V., Wegeng, R.S., 2000. Solvent extraction and gas absorption using microchannel contactors. In: Ehrfeld, W. (Ed.), Microreaction Technology: Industrial Prospects: IMRET 3: Proceedings of the Third International Conference on Microreaction Technology. Springer, Berlin, pp. 541–549.

Tomida, T., Yusa, F., Okazaki, T., 1978. Effective interfacial area and liquid-side mass transfer coefficient in the upward two-phase flow of gas–liquid mixtures. Chemical Engineering Journal 16, 81–88.

Tortopidis, P., Bontozoglou, V., 1997. Mass transfer in gas–liquid flow in small-diameter tubes. Chemical Engineering Science 52, 2231–2237.

Triplett, K.A., Ghiaasiaan, S.M., Abdel-Khalik, S.I., Sadowski, D.L., 1999a. Gas–liquid two-phase flow in microchannels Part I: two-phase flow patterns. International Journal of Multiphase Flow 25, 377–394.

Triplett, K.A., Ghiaasiaan, S.M., Abdel-Khalik, S.I., Lemouel, A., McCord, B.N., 1999b. Gas–liquid two-phase flow in microchannels Part II: void fraction and pressure drop. International Journal of Multiphase Flow 25, 395–410.

Vandu, C.O., Liu, H., Krishna, R., 2005. Mass transfer from Taylor bubbles rising in single capillaries. Chemical Engineering Science 60, 6430–6437.

Wambsganss, M.W., Jendrzejczyk, J.A., France, D.M., Obot, N.T., 1992. Frictional pressure-gradients in two-phase flow in a small horizontal rectangular channel. Experimental Thermal and Fluid Science 5, 40–56.

Wang, C.C., Chiang, C.S., Lu, D.C., 1997. Visual observation of two-phase flow pattern of R-22, R-134a, and R-407C in a 6.5-mm smooth tube. Experimental Thermal and Fluid Science 15, 395–405.

Watts, P., Haswell, S.J., 2005. The application of micro reactors for organic synthesis. Chemical Society Reviews 34, 235–246.

Yeong, K.K., Gavriilidis, A., Zapf, R., Hessel, V., 2004. Experimental studies of nitrobenzene hydrogenation in a microstructured falling film reactor. Chemical Engineering Science 59, 3491–3494.

Yue, J., Chen, G., Yuan, Q., 2004. Pressure drops of single and two-phase flows through T-type microchannel mixers. Chemical Engineering Journal 104, 11–24.

Yue, J., Chen, G., Yuan, Q., Luo, L., Le Gall, H., 2006. Mass transfer in gas–liquid flow in microchannels. Journal of Chemical Industry and Engineering (China) 6, 1296–1303.

Zanfir, M., Gavriilidis, A., Wille, Ch., Hessel, V., 2005. Carbon dioxide absorption in a falling film microstructured reactors: experiments and modeling. Industrial & Engineering Chemistry Research 44, 1742–1751.

Zhao, T.S., Bi, Q.C., 2001a. Cocurrent air-water two-phase flow patterns in vertical triangular microchannels. International Journal of Multiphase Flow 27, 765–782.

Zhao, T.S., Bi, Q.C., 2001b. Pressure drop characteristics of gas–liquid two-phase flow in vertical miniature triangular channels. International Journal of Heat and Mass Transfer 44, 2523–2534.